Touseef Fayaz[1], *Olumuyiwa Otegbeye*[2], *Md. Sharifuddin Ansari*[1], *Mumukshu Trivedi*[3*]

JEFFREY NANOFLUID FLUID FLOW INDUCED DUE TO THE IMPULSIVE MOVEMENT OF RIGA PLATE

STRUJANJE JEFFREY NANOFLUIDA INDUKOVANOG IMPULSNIM KRETANJEM RIGA PLOČE

Originalni naučni rad / Original scientific paper
Rad primljen / Paper received: 15.07.2024
https://doi.org/10.69644/ivk-2025-siA-0093

Adresa autora / Author's address:
[1)] School of Technology, Pandit Deendayal Energy University, Gandhinagar, India
[2)] School of Computer Science and Applied Mathematics, Faculty of Science, University of the Witwatersrand, Johannesburg, Gauteng, South Africa
[3)] Institute of Management, Nirma University, Ahmedabad, Gujarat, India [*]email: mumukshutrivedi@nirmauni.ac.in

Keywords
- convective boundary condition
- Jeffrey nanofluid
- spectral quasilinearization method
- Riga plate, impulsive movement
- activation energy

Ključne reči
- granični uslov konvekcije
- Jeffrey nanofluid
- metoda spektralne kvazilinearizacije
- Riga ploča, impulsno kretanje
- energija aktivacije

Abstract

Unsteady flow, induced by an impulsive movement of boundary, of Jeffrey nanofluid over surface having the ability to bring about electromagnetic hydrodynamic behaviour is studied. Integrated effects of magnetic field, modified Lorentz force, viscous dissipation, thermophoresis, Brownian motion, activation energy and convective boundary conditions are considered in the present flow analysis. Mathematical replica of the flow system in terms of system of nonlinear and coupled partial differential equations is solved using spectral quasilinearization recipe. Solutions obtained by this method are substituted in the original system of equations and a very good outcome is achieved. A detailed study on the effects of some selected flow parameter is performed by replicating the solutions in graphical form. Expressions of Nusselt and Sherwood number are presented.

Izvod

U radu se proučava nestacionarno strujanje Jeffrey nanofluida preko površine koja izaziva elektromagnetno hidrodinamičko ponašanje, gde je strujanje indukovano impulsnim kretanjem granične površine. U analizi strujanja razmatraju se integrisani uticaji magnetnog polja, modifikovane Lorencove sile, viskoznog trenja, termoforeze, Braunovog kretanja, energije aktivacije i graničnih uslova konvekcije. Matematički model sistema strujanja opisan sistemom nelinearnih i spregnutih parcijalnih diferencijalnih jednačina se rešava primenom metode spektralne kvazilinearizacije. Smenom dobijenih rešenja u početni sistem jednačina postiže se veoma dobar ishod. Rešenja dobijena grafički doprinose detaljnom proučavanju uticaja pojedinih izabranih parametara strujanja. Dati su i izrazi za Nuseltov i Šervudov broj.

INTRODUCTION

Nanofluid takes a very crucial position in the field of science and engineering owing to its enhanced thermal conductivity. Some of fascinating applications of nanofluid include innovating new generation of cooling technology, solar thermal systems, biomedical science, heat exchangers, thermal energy transport, metal working processes, textile industry and food processing, etc. Additionally, the effects of heat transfer mediated by nanofluids have great effects across the research and industrial sectors. The impact of nanofluids has been enormous, in the field of industrial applications such as spanning discs, plates, parallel plates, cylinders, parallel discs, stretching sheets, stretching discs, cones, or channels in both rotating and non-rotating environments. Gupta et al. /1/ remarked on interplay of magnetic fields, mixed convection, radiation, and chemical reactions within the context of non-Newtonian nanofluid dynamics. Shafiq et al. /2/ presented the fascinating realm of Casson Marangoni-driven forced convection in nanofluids, near an infinite disk under inclined magnetic field. Rasool and Zhang /3/ ventured into the Cattaneo-Christov models, shedding light on the heat and mass diffusion in nanofluids near nonlinear stretching sheet coursing through non-Darcian porous media. Rasool et al. /4/ shredded some light on the mechanics behind forced convection flow in second-grade nanofluids, considering the Lorentz force and Marangoni effects. Contribution by Lund et al. /5/ explored the stability of Casson nanofluid flows at an exponentially shrinking surface in Darcy Forchheimer porous media. Nayak et al. /6/ studied the multifaceted effects of momentum, thermal, and solutal slips at electromagnetic sheets experiencing stagnation flows of Walters' B nanofluids. This analysis incorporates the Cattaneo-Christov flux concept on heat and mass diffusion. The effects of an elevated magnetic field, non-uniform heat source/sink and chemical reaction on viscous dissipative and radiative unsteady flow of a Williamson nanofluid across a vertical extending porous surface are well demonstrated in /7/. The characteristics of heat transfer on viscous dissipative flow of Jeffrey nanofluid, induced due to impulsive movement of plate with the impact of activation energy was reported by Trivedi et al. /8/. Casson nanofluid comprising the combined effects of Hall current, activation energy, externally heat source/sink and radiation was simulated numerically by Kumar et al. /9/.

In addition to the aforementioned geometrical constructions, the Riga plate or electromagnetic actuator, which is an outcome of pioneer work by Gailitis and Lielausis /10/, is a tool that can generate Lorentz force along a boundary wall. A magnetic and electric field produced by the Riga plate, made up of alternate positioning of electrodes and magnets in span-wise aligned arrays, increase the Lorentz force in the fluid flow direction. Riga plate counterbalances fluid flow close to boundary layer. Electromagnetic force, in addition to wall motion and suction, controls fluid flow. Applying an electrical field is beneficial for effective flow control because a magnetic field does not generate enough currents when weakly conducting fluids are involved. Riga plate minimizes boundary layer separation, skin friction, and pressure drag on submarines. Magnetic force-driven flows across the Riga plate are important in a variety of industrial and engineering operations. Hayat et al. /11/ studied the properties of heat transfer of nanofluid flow induced by the convectively heated Riga surface taking into account heat generation/absorption effects. Rasool et al. /12/, conducted an analysis on the behaviour of second grade nanofluid flows at a vertically heated Riga plate. Shamshuddin et al. /13/ explored the influence of absorption and Joule heating on magnetohydrodynamic (MHD) flow between Riga plates, considering the Cattaneo-Christov heat flux. Hakeem et al. /14/ examined the influence of nonlinear thermal radiation on 3-dimensional flow of nanofluid consisting base fluid as water and sodium alginate and nanoparticle as aluminium oxide and magnetite, adjacent to a Riga plate. Ragupathi et al. /15/ examined the probability of achieving distinct findings by comparing FeO_4/Al_2O_3 nanoparticles with $H_2O/NaC_6H_9O_7$ as base nanofluids over the Riga plate with irregular heat source/sink effects. Iqbal et al. /16/ studied the effects of viscous dissipation, thermal radiation, and melting heat on stagnation point flow across the Riga surface. This study shows that melting heat transfer has direct relation with radiation parameter and inverse relation with temperature distribution. Rida et al. /17/ investigated the process of heat transfer in nanofluid flow past a vertical convectively heated Riga plate under zero normal wall mass flux condition. Papers /18-24/ explore various aspects of nanofluid flow over Riga surface. Nasir et al. /25/ investigated the characteristics of two base fluids, namely, H_2O and $C_2H_6O_2$ and TiO_2 nanoparticle in unsteady electromagnetohydrodynamic nanofluid flow over Riga plate with radiation. It was revealed that nanofluid consisting of $C_2H_6O_2$ as base fluid possesses improved heat transfer than nanofluid with H_2O as base fluid. Alhowaity et al. /26/ analysed the consequences of activation energy and heat generation on radiative flow of a nanofluid at convected vertical Riga plate employing zero mass flux and convectively heated surface. Algehyne et al. /27/ investigated effects of magnetic field, microorganism, activation energy and heat source/sink on flow of hybrid MgO-Ag water nanoliquid at Riga plate allowing slip at boundary surface. Aamir et al. /28/ discussed the flow properties of an Al_2O_3-Cu water hybrid nanofluid via a Riga plate integrating the factors like heat flux, suction, viscous dissipation, entropy generation, convective and slippage condition at the bounding surface. Riaz et al. /29/ reported an analysis on heat and mass transfer, using Cattaneo-Christov model, of ZnO-SAE50 nanolubricant in a Darcy Forchheimer medium past a Riga plate. Ansari et. al. /30/ made an effort to describe the Jeffrey nanofluid flow phenomenon on a Riga plate by incorporating the effects of inconsistent heat source/sink and viscous dissipation. Ramanjini et al. /31/ examined the two-dimensional time dependent boundary layer mixed convective and radiative horizontally stretched flow of a Williamson nanofluid over a Riga plate.

A widespread literature survey reveals that a study pertaining to unsteady Jeffrey (rate type) nanofluid flow, generated by impulsive movement of a Riga surface with convective conditions doesn't exist. This work explores the unsteady flow of Jeffery nanofluid flow over surface that can exhibit electromagnetic hydrodynamic behaviour when the boundary is moved impulsively. The combined effects of a magnetic field, modified Lorentz force, viscous dissipations, thermophoresis, Brownian motion, activation energy and convective boundary conditions are taken into consideration in the analysis of heat transfer. The PDEs used to model this problem were numerically solved using the spectral quasilinearization technique. Mathematica® and MATLAB® were used to generate approximate solutions. Convergence and accuracy of numerical scheme were substantiated by evaluating the solution error and residual error, in respect. These assessments show a satisfactory outcome. The approximate results are displayed in graphical form to examine the insight of flow, temperature, and nanoparticle concentration pattern.

MATHEMATICAL FORMULATION OF THE PROBLEM

An unsteady flow across an electromagnetic surface, Riga surface, considering the surface along η direction where ξ direction is considered normal to the surface. The unsteady nature of the flow and Jeffrey nanofluid is considered. The following points are considered while modelling the flow system.

1. Flow properties are dependent only on ξ direction and time.
2. $\hat{\phi}_{1\infty}$ and $\hat{\phi}_{2\infty}$ are fluid temperature and nanoparticle concentration outside the boundary layer region.
3. Magnetic field of constant strength is applied in the ξ direction.
4. Induced magnetic field is neglected.
5. Arrhenius activation energy is considered.
6. Flow is induced by impulsive movement of the electromagnetic surface.

Figure 1 is the pictorial representation of the flow system.

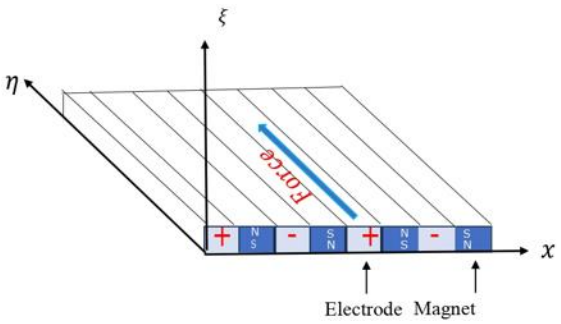

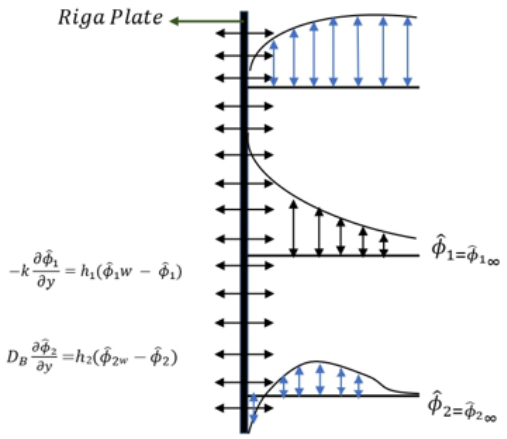

Figure 1. Schematic diagram of Jeffrey nanofluid over Riga plate.

Under the above mentioned points, Eqs.(1)-(3) are the mathematical representation of this problem.

$$\partial_{\hat{t}}\hat{v}_1=\nu b^{-1}(1+\lambda_2\partial_{\hat{t}})\partial_{\xi\xi}\hat{v}_1-\sigma\rho^{-1}B^2\hat{v}_1+\frac{\pi j_0M_0}{8\rho}e^{\pi a^{-1}\xi}, \quad (1)$$

$$\partial_{\hat{t}}\hat{\phi}_1=\alpha\partial_{\xi\xi}\hat{\phi}_1+\tau\left[D_B\partial_\xi\hat{\phi}_2\partial_\xi\hat{\phi}_1+D_{\hat{\phi}_1}(\hat{\phi}_{1\infty})^{-1}(\partial_\xi\hat{\phi}_1)^2\right]+$$
$$+\mu(\rho c_p b)^{-1}\left[(\partial_\xi\hat{v}_1)^2+\lambda_2\partial_\xi\hat{v}_1\partial_{\hat{t}\xi}\hat{v}_1\right], \quad (2)$$

$$\partial_{\hat{t}}\hat{\phi}_2=D_B\partial_{\xi\xi}\hat{\phi}_2-k_r^2(\hat{\phi}_1)^n(\hat{\phi}_{1\infty})^{-n}e^{-E_a(k\hat{\phi}_1)^{-1}}(\hat{\phi}_2-\hat{\phi}_{2\infty})+$$
$$+D_{\hat{\phi}_1}(\hat{\phi}_{1\infty})^{-1}\partial_{\xi\xi}\hat{\phi}_1, \quad (3)$$

where: parameters a, B, σ, j_0, M_0 are respectively, width of magnets between electrodes, applied magnetic field strength, electrical conductivity, current density in electrode, and the magnetization of magnets mounted on the surface of Riga plate. Parameters $\hat{v}_1,\hat{\phi}_1,\hat{\phi}_2,\hat{\phi}_{1\infty},\hat{\phi}_{2\infty}$, λ_1, λ_2, $(\rho c)_f$, D_B, , k_r^2, E_a, $D_{\hat{\phi}_1}$, and τ are, respectively, fluid velocity in η-direction, fluid temperature, nanoparticle concentration, ambient temperature, ambient concentration, ratio of relaxation to retardation time, relaxation time, kinematic viscosity, density of base fluid, specific heat at constant pressure, effective heat capacity of the nanoparticle material, heat capacity of the fluid, Brownian diffusion coefficient, thermophoresis diffusion coefficient, chemical reaction rate constant, activation energy, and a parameter defined by ratio $(\rho c)_p/(\rho c)_f$. The term $k_r^2(\hat{\phi}_1)^n(\hat{\phi}_{1\infty})^{-n}e^{-E_a(k\hat{\phi}_1)^{-1}}(\hat{\phi}_2-\hat{\phi}_{2\infty})$ symbolizes transfigured Arrhenius function, where n is a constant exponent. Also $b = 1 + \lambda_1$. The pressure gradient and external forces are neglected in momentum equation.

Boundary conditions:

$$\hat{t}=0:\ \forall\xi;\ \hat{v}_1=0,\ \hat{\phi}_1=0,\ \hat{\phi}_2=0, \quad (4)$$

$$\hat{t}>0:\begin{cases}\text{at}\quad \xi=0:\quad \hat{v}_1=v_0;\quad -k\partial_\xi\hat{\phi}_1=h_1(\hat{\phi}_{1w}-\hat{\phi}_1)\\ -D_B\partial_\xi\hat{\phi}_2=h_2(\hat{\phi}_{2w}-\hat{\phi}_2)\\ \text{as}\quad \xi\to\infty:\quad v_1\to0;\quad \hat{\phi}_1\to0;\quad \hat{\phi}_2\to0\end{cases} \quad (5)$$

where: $\hat{v}_1$ denotes velocity in η direction; h_1 is the surface heat transfer coefficient; h_2 is wall mass transfer coefficient. Equations (1)-(3) can be transformed into equivalent partial differential equations using the technique of similarity solutions. We introduce the following dimensionless variables:

$$v=\hat{v}_1/v_0,\ \ y=\xi/\xi_0,\ \ \xi_0=\nu/v_0,\ \ t=\hat{t}/\hat{t}_0,\ \ \hat{t}_0=\nu/v_0^2,$$
$$\phi_1=(\hat{\phi}_1-\hat{\phi}_{1\infty})/(\hat{\phi}_{1w}-\hat{\phi}_{1\infty}),\ \ \phi_2=(\hat{\phi}_2-\hat{\phi}_{2\infty})/(\hat{\phi}_{2w}-\hat{\phi}_{2\infty}). \quad (6)$$

Using Eq.(6) in Eqs.(1)-(3), the non-dimensional system is:

$$\partial_{yy}v+\lambda(\partial_t\partial_{yy}v)-b\partial_tv+bQe^{-\beta y}-bMv=0, \quad (7)$$

$$-\partial_t\phi_1+N_{\phi_1}(\partial_y\phi_1)^2+\mathrm{Ec}b^{-1}[(\partial_yv)^2+\lambda\partial_yv\partial_{ty}v]+$$
$$+(\mathrm{Pr})^{-1}\partial_{yy}\phi_1+N_b\partial_y\phi_2\partial_y\phi_1=0, \quad (8)$$

$$\partial_{yy}\phi_2-\mathrm{Le}\partial_t\phi_2-\mathrm{Le}k(\phi_1\delta+1)^ne^{-E(\phi_1\delta+1)^{-1}}\phi_2+$$
$$+N_{\phi_1}(N_b)^{-1}\partial_{yy}\phi_1=0, \quad (9)$$

and the transformed conditions are

$$\text{at } t=0 \text{ and } \forall y>0:\ v(y,0)=0,\ \phi_1(y,0)=0,\ \phi_2(y,0)=0,$$
$$\text{at } y=0 \text{ and } \forall t>0:\ \partial_y\phi_1=-\Gamma_1(1-\phi_1),\ \partial_y\phi_2=-\Gamma_2(1-\phi_2),$$
$$\text{as } y\to\infty \text{ and } \forall t>0:\ v(\infty,t)\to0;\ \phi_1\to0;\ \phi_2\to0, \quad (10)$$

where:

$$M=\sigma B^2/\rho\nu,\ \lambda=\lambda_2v_0^2/\nu,\ Q=\pi j_0M_0/8\rho\nu,\ \beta=\pi\nu/av_0,$$
$$\mathrm{Pr}=\nu/\alpha,\ \delta=(\phi_{1w}-\phi_{1\infty})/\phi_{1\infty},\ N_b=\tau D_B(\phi_{2w}-\phi_{2\infty})/\nu,$$
$$N_{\phi_1}=\tau D_{\phi1}(\phi_{1w}-\phi_{1\infty})/\nu\phi_{1\infty},\ k=k_r^2\nu/v_0^2,\ \mathrm{Le}=\nu/D_B,$$
$$\mathrm{Ec}=v_0^2/\nu(\phi_{1s}-\phi_{1\infty}),\ \alpha=k/(\rho c)_f,\ E=E_a/k\phi_{1\infty},$$

where: M, Q, β, Pr, N_b, $N_{\phi1}$, Le, Ec, E, and Γ_i (i = 1, 2, 3) are respectively, magnetic parameter, modified Hartmann number, dimensionless constant, Prandtl number, Brownian motion parameter, thermophoresis parameter, Lewis number, Eckert number, activation energy parameter and Biot numbers.

Nusselt number Nu_x and Sherwood number Sh_x, are presented as: $\mathrm{Nu}_x=-\partial_y\phi_1\big|_{y=0}$, $\mathrm{Sh}_x=-\partial_y\phi_2\big|_{y=0}=0$.

SOLUTION TECHNIQUE

The Eqs. (7) to (9) are nonlinear and coupled, making it generally hard to find an analytical solution. Here, we will go through SQLM method and use it to arrive at a numerical solution for systems Eqs.(7)-(9) under boundary conditions Eq.(10). In order to force the system of equations to be solved, it is initially figured that the system consists of separate equations for v, ϕ_1, and ϕ_2. The approximate solutions of each function and their derivatives at successive iteration levels (i.e., at $(r + 1)^{\text{th}}$ and r^{th} level, r is iteration level) differ slightly, hence a quasilinearization technique employing Taylor series expansion is used to linearize the resolved equations. By using the Chebyshev spectral collocation method, the linear resolved system of equations is solved. Nonlinear terms in the system of Eqs. (7)-(9) are $\partial_y\phi_1\partial_y\phi_2$, $(\partial_y\phi_1)^2$, $(\partial_yv)^2$, $\partial_yv\partial_{ty}{}^2v$, $(1 + \phi_1\delta)^n$, and $(1 + \phi_1\delta)^{-1}$, δ is the temperature difference parameter.

First, we convert Eqs.(7)-(9) into quasilinear form as:

$$v''_{r+1}+[a_1]v_{r+1}=-\lambda\partial_tv''_{r+1}+b\partial_tv_{r+1},$$
$$[b_1]v'_{r+1}+\frac{1}{\mathrm{Pr}}\phi''_{1r+1}+[b_2]\phi'_{1r+1}+[b_3]\phi'_{2r+1}=$$
$$=[b_4]\partial_tw'_{r+1}+\partial_t\phi_{1r+1}+b_5,$$
$$N_{\phi_1}(N_b)^{-1}\phi''_{1r+1}+[c_1]\phi_{1r+1}+\phi''_{2r+1}+[c_2]\phi_{2r+1}=$$
$$=\mathrm{Le}\partial_t\phi_{2r+1}+c_3, \quad (11)$$

where the iteration levels for the current and previous iterations are indicated by subscripts $r + 1$ and r and

$$a_1=-bM,\ b_1=2\mathrm{Ec}b^{-1}v_r'+\lambda\,\mathrm{Ec}b^{-1}\partial_t v_r',$$
$$b_2=N_b\phi_{2r}'+2N_{\phi_1}\phi_{1r}',\ b_3=N_b\phi_{1r}',\ b_4=-\lambda\,\mathrm{Ec}b^{-1}v_r',$$
$$b_5=N_b\phi_{1r}'\phi_{2r}'+N_{\phi_1}\phi_{1r}'^2+\mathrm{Ec}b^{-1}v_r'^2+\lambda\,\mathrm{Ec}b^{-1}v_r'\partial_t v_r',$$
$$c_1=-\mathrm{Le}K\phi_{2r}\delta\exp(-E(1+\phi_{1r}\delta)^{-1})[n(\phi_{1r}\delta+1)^{n-1}+E(\phi_{1r}\delta+1)^{n-2}],$$
$$c_2=-\mathrm{Le}K(\phi_{1r}\delta+1)^n\exp(-E(1+\phi_{1r}\delta)^{-1}),$$
$$c_3=-\mathrm{Le}K\exp(-E(1+\phi_{1r}\delta)^{-1})\{(\phi_{1r}\delta+1)^n+\phi_{2r}\phi_{1r}\delta\times$$
$$\times[n(\phi_{1r}\delta+1)^{n-1}+E(\phi_{1r}\delta+1)^{n-2}]\}. \quad (12)$$

where: K is a chemical reaction parameter.

Chebyshev collocation spectral method is used to solve the system Eqs.(13)-(15), for this the space and the time domain is transformed to [-1, 1] by using linear transformation. Bivariate Lagrange interpolation polynomials are used to govern approximate solution, which is defined as

$$Y(y,t)\approx\sum_{i=0}^{M_y}\sum_{j=0}^{M_t}Y(y_i,t_j)L_i(y)L_j(t),\quad F=(v,\phi_1,\phi_2), \quad (13)$$

which interpolates unknowns: fluid velocity, temperature and concentration at Gauss-Lobatto collocation points, defined as

$$y_i=\cos\left(\frac{\pi i}{M_y}\right),\ t_j=\cos\left(\frac{\pi j}{M_t}\right),\ i=0,1,\ldots,M_y,\ j=0,1,\ldots,M_t$$

Chebyshev differentiation matrices D, d with respect to y (space variable) and t (time variable) of order $(M_y+1)\times(M_y+1)$ and $(M_t+1)\times(M_t+1)$, respectively, are taken as

$$\left.\frac{\partial^m Y}{\partial y^m}\right|_{(y_k,t_i)}=\mathbf{D}^m\mathbf{Y}_i,\quad m=1,2,3\ ,\ \left.\frac{\partial Y}{\partial t}\right|_{(y_k,t_i)}=\sum_{j=0}^{M_y}\mathbf{d}_{ij}\mathbf{Y}_j\ . \quad (14)$$

Thus $\mathbf{Y}_i$ represents $\mathbf{Y}_i=[Y_i(y_0),Y_i(y_1),\ldots,Y_i(y_{M_y})]^T$. (15)

The system Eq.(11) which is now linearized, is divided into smaller disjoint intervals $\rho_s=[t_{s-1},\ t_s]$, $s=1,\ 2,\ \ldots,\ T$, where $T\in\rho$, $\rho=[0,\ T]$ by breaking up the time interval t. The fundamental principle of the multi-domain method is highlighted by this splitting process. The approach is used to find solutions to the problem inside the first subinterval by starting with an initial solution that fulfils the boundary conditions of the system of partial differential equations. Once the system of equations has been solved in all subintervals, the resulting solutions are used as initial solutions in the following sub-interval. A continuity condition can be used to express this as

$$Y^{(\varepsilon)}(y,t_{\varepsilon-1})=F^{(\varepsilon-1)}(y,t_{\varepsilon-1})\,. \quad (16)$$

The system Eq.(11) assumes the form after the multi-domain approach is used as

$$v_{r+1}''^{\varepsilon}+(a_1)v_{r+1}^{(\varepsilon)}=-\lambda\partial_t v_{r+1}''^{\varepsilon}+b\partial_t v_{r+1}^{(\varepsilon)},$$
$$[b_1^{(\varepsilon)}]v_{r+1}'^{(\varepsilon)}+\frac{1}{\mathrm{Pr}}\phi_{1r+1}''^{(\varepsilon)}+[b_2^{(\varepsilon)}]\phi_{1r+1}'^{(\varepsilon)}+[b_3^{(\varepsilon)}]\phi_{2r+1}'^{(\varepsilon)}=$$
$$=[b_4^{(\varepsilon)}]\partial_t v_{r+1}'^{(\varepsilon)}+\partial_t\phi_{1r+1}^{(\varepsilon)}+b_5^{(\varepsilon)},$$
$$N_{\phi_1}(N_b)^{-1}\phi_{1r+1}''^{(\varepsilon)}+[c_1^{(\varepsilon)}]\phi_{1r+1}^{(\varepsilon)}+\phi_{2r+1}''^{(\varepsilon)}+[c_2^{(\varepsilon)}]\phi_{2r+1}^{(\varepsilon)}=$$
$$=\mathrm{Le}\,\partial_t\phi_{2r+1}^{(\varepsilon)}+c_3^{(\varepsilon)}. \quad (17)$$

By applying the Chebyshev spectral method on the linearized system of Eqs.(17), we obtain

$$\mathbf{A}_{11,i}^{(\varepsilon)}(\mathbf{v})_{r+1,i}^{(\varepsilon)}+\mathbf{A}_{12,i}^{(\varepsilon)}(\mathbf{\Phi_1})_{r+1,i}^{(\varepsilon)}+\mathbf{A}_{13,i}^{(\varepsilon)}(\mathbf{\Phi_2})_{r+1,i}^{(\varepsilon)}+$$
$$+\lambda\sum_{j=0}^{M_y}\mathbf{d}_{i,j}\mathbf{D}^2\mathbf{v}_{r+1,j}^{(\varepsilon)}-b\sum_{j=0}^{M_y}\mathbf{d}_{i,j}\mathbf{v}_{r+1,j}^{(\varepsilon)}=\mathbf{R}_{1,i}^{(\varepsilon)}, \quad (18)$$

$$\mathbf{A}_{21,i}^{(\varepsilon)}(\mathbf{v})_{r+1,i}^{(\varepsilon)}+\mathbf{A}_{22,i}^{(\varepsilon)}(\mathbf{\Phi_1})_{r+1,i}^{(\varepsilon)}+\mathbf{A}_{23,i}^{(\varepsilon)}(\mathbf{\Phi_2})_{r+1,i}^{(\varepsilon)}-[\mathbf{b}_{4,i}^{(\varepsilon)}]\times$$
$$\times\sum_{j=0}^{M_y}\mathbf{d}_{i,j}\mathbf{D}\mathbf{v}_{r+1,j}^{(\varepsilon)}-\sum_{j=0}^{M_y}\mathbf{d}_{i,j}(\mathbf{\Phi_1})_{r+1,j}^{(\varepsilon)}=\mathbf{R}_{2,i}^{(\varepsilon)}, \quad (19)$$

$$\mathbf{A}_{31,i}^{(\varepsilon)}\mathbf{v}_{r+1,i}^{(\varepsilon)}+\mathbf{A}_{32,i}^{(\varepsilon)}(\mathbf{\Phi_1})_{r+1,i}^{(\varepsilon)}+\mathbf{A}_{33,i}^{(\varepsilon)}(\mathbf{\Phi_2})_{r+1,i}^{(\varepsilon)}-$$
$$-\mathrm{Le}\sum_{j=0}^{M_y}\mathbf{d}_{i,j}(\mathbf{\Phi_2})_{r+1,j}^{(\varepsilon)}=\mathbf{R}_{3,i}^{(\varepsilon)}, \quad (20)$$

where: $\mathbf{A}_{11,i}^{(\varepsilon)}=\mathbf{D}^2+(a_1)\mathbf{I}$, $\mathbf{A}_{12,i}^{(\varepsilon)}=\mathbf{A}_{13,i}^{(\varepsilon)}=0$, $\mathbf{A}_{21,i}^{(\varepsilon)}=[\mathbf{b}_1^{(\varepsilon)}]\mathbf{D}$, $\mathbf{A}_{22,i}^{(\varepsilon)}=\frac{1}{\mathrm{Pr}}\mathbf{D}^2+[\mathbf{b}_2^{(\varepsilon)}]\mathbf{D}$, $\mathbf{A}_{13,i}^{(\varepsilon)}=[\mathbf{b}_3^{(\varepsilon)}]\mathbf{D}$, $\mathbf{A}_{31,i}^{(\varepsilon)}=\mathbf{0}$, $\mathbf{A}_{32,i}^{(\varepsilon)}=N_{\phi_1}(N_b)^{-1}\mathbf{D}^2+[c_1^{(\varepsilon)}]$, $\mathbf{A}_{33,i}^{(\varepsilon)}=\mathbf{D}^2+[\mathbf{c}_2^{(\varepsilon)}]$ and $\mathbf{I}$ is an identity matrix of size $(M_y+1)\times(M_y+1)$.

CONVERGENCE AND ACCURACY

This section describes the accuracy of convergent solutions obtained with SQLM as well as the convergence of solutions. Figures 2-10 demonstrate the accuracy of the numerical scheme and convergence for $N_b=0.1$, $N_t=0.1$, Le = 10, $\delta=1$, $E=0.05$, Pr = 12, $M=3$, Ec = 0.2, $n=1$, $K=1$, $\lambda=0.1$, $\lambda_1=0.1$, and $Q=1$. In y (space) direction 80 gridpoints in t (time) are used. The results of grid-independent test show that these are capable of producing accurate solutions.

Solution error analysis

When $Q=1$, $N_b=0.1$, $N_t=0.1$, Le = 10, $\delta=1$, $E=0.05$, Pr = 12, $M=3$, Ec = 0.2, $n=1$, $K=1$, $\lambda=0.1$, and $\lambda_1=0.1$, by calculating the error derived from the solutions of two successive iterations and taking the infinity norm, convergence of the SQLM test is accomplished,

$$\|v\|_\infty=\max_{0\le i\le M_y}\left\|v_{r+1,i}-v_{r,i}\right\|_\infty, \quad (21)$$

, (22)

. (23)

When the error between successive solutions becomes consistent to a defined number of significant digits, indicating that additional increases in the number of iterations have no effect on the corresponding solutions, the approximate solution achieved using the SQLM is said to have converged. Figures 2-4 display solution errors of the system of PDEs. The solution error shows a monotonic decline as the number of iterations rises, demonstrating the convergence of the solution approach. It can be seen that the error reduces to 10^{-14} just after the few iterations and remains consistent for v while it takes almost 6 iterations for convergence to occur for ϕ_1 to 10^{-14} and ϕ_2 to 10^{-13}. This solution error analysis confirms a quick convergence of solution method in a lower number of iterations,

, (24)

, (25)

. (26)

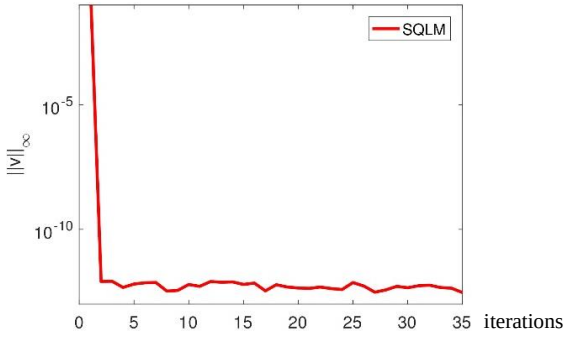

Figure 2. Solution error of ν with iteration.

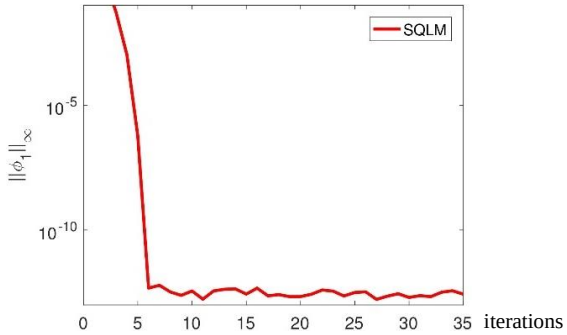

Figure 3. Trend of solution error of ϕ_1 with iteration.

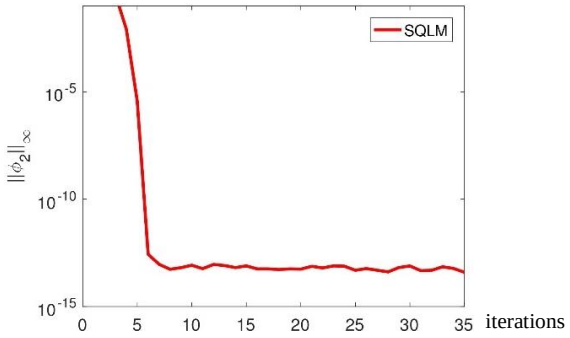

Figure 4. Solution error of ϕ_2 with iteration.

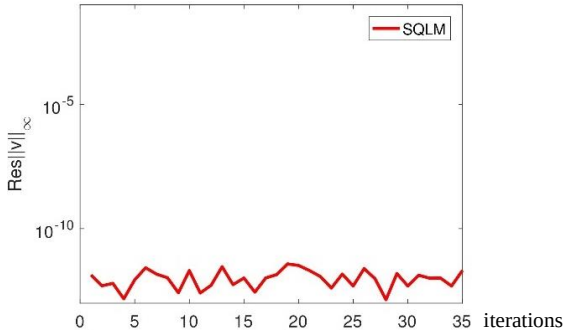

Figure 5. Residual error of ν with iteration.

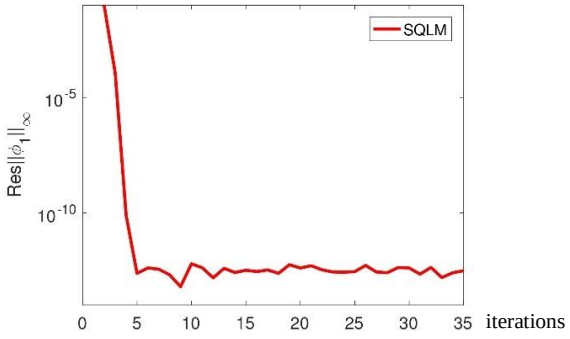

Figure 6. Residual error of ϕ_1 with iteration.

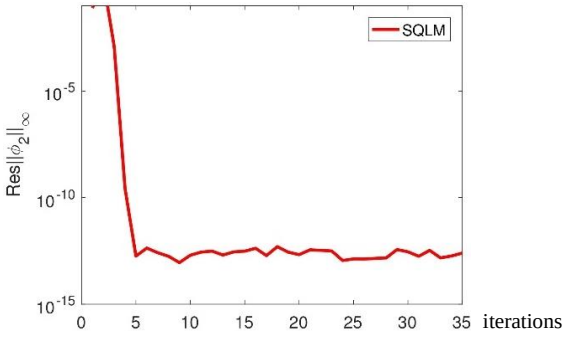

Figure 7. Residual error of ϕ_2 with iteration.

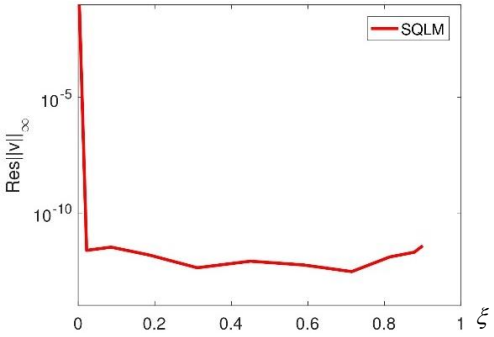

Figure 8. Residual error behaviour of ν with ξ.

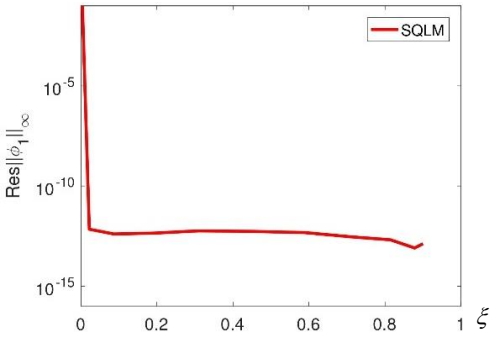

Figure 9. Residual error behaviour of ϕ_1 with ξ.

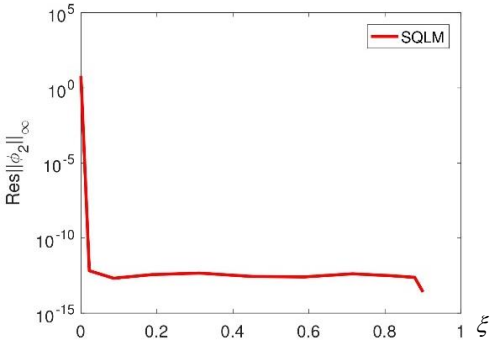

Figure 10. Residual error behaviour of ϕ_1 with ξ.

RESULTS AND DISCUSSION

This section emphasizes to assess the behaviour of physical parameters on fluid velocity v, temperature ϕ_1, and nanoparticle concentration ϕ_2 in the boundary layer region. The following values of parameters, i.e., $M = 3$, $\mathrm{Pr} = 12$, $\delta = 1$, $N_b = 0.1$, $N_t = 0.1$, $E = 0.05$, $\lambda = 0.1$, $\lambda_1 = 0.1$, $\mathrm{Le} = 10$, $n = 1$, $k = 1$, $\mathrm{Ec} = 0.2$, $\beta = 0.5$, $\Gamma_1 = 2$, $\Gamma_2 = 1$, and $Q = 1$ are utilised to generate the graphs.

An impact of parameter β on the velocity profile near the boundary layer region is picturised in Fig. 11. An upsurge in β reveals a decline in velocity profile.

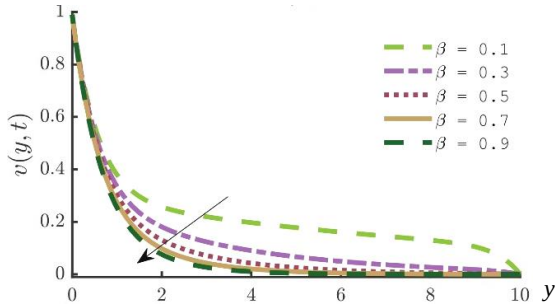

Figure 11. Impact of β on fluid velocity.

Figures 12-15 witness the influence of Biot numbers on the temperature and concentration profiles. Improvement in convective heat and mass transfer coefficient shows an elevation in fluid temperature as well as nanoparticle concentration profiles near the bounding surface. Fluid temperature and nanoparticle concentration drop uniformly along η to adhere the free stream values. Nanoparticle concentration grows near the wall on account of sedimentation. This happens because of the convectively heated boundary surface.

Figures 16-18 show the response of modified Hartmann number on fluid velocity, temperature profile, and nanoparticle concentration. Since Riga plate produces electromagnetic waves and this electromagnetic force acts along the fluid motion, this helps to enhance fluid velocity and concentration profiles. This fact is revealed from the Figs. 16 and 18. Modified Hartman number exerts a diminishing influence in fluid temperature, i.e., a boost in heat transfer (Fig. 17).

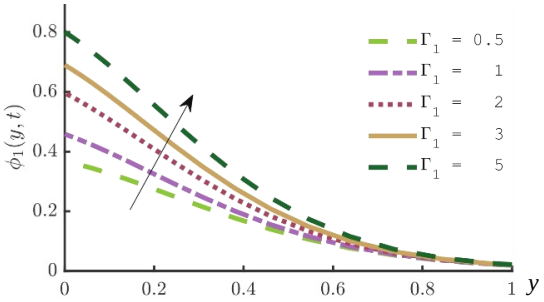

Figure 12. Effect of Γ_1 on temperature field.

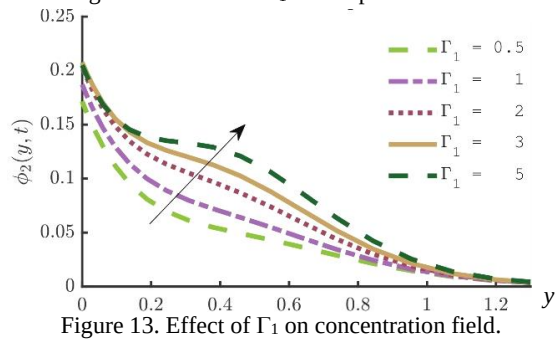

Figure 13. Effect of Γ_1 on concentration field.

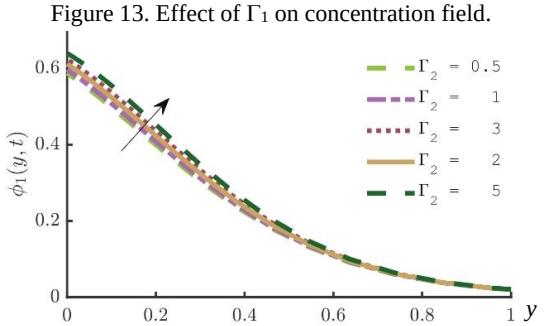

Figure 14. Impact of Γ_2 on temperature field.

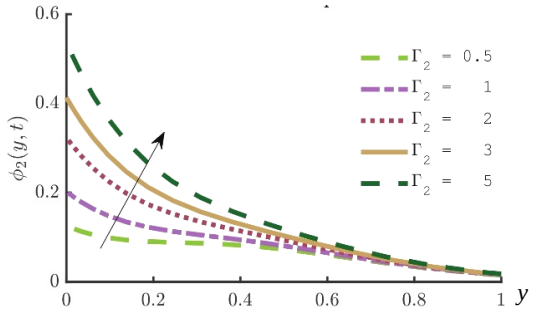

Figure 15. Impact of Γ_2 on concentration field.

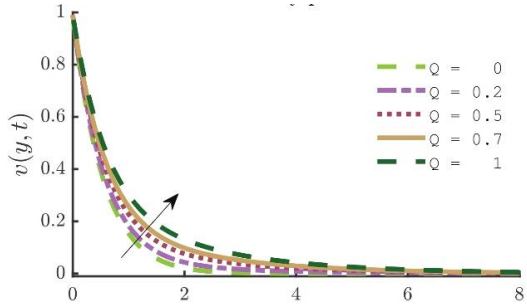

Figure 16, Impact of Q on velocity.

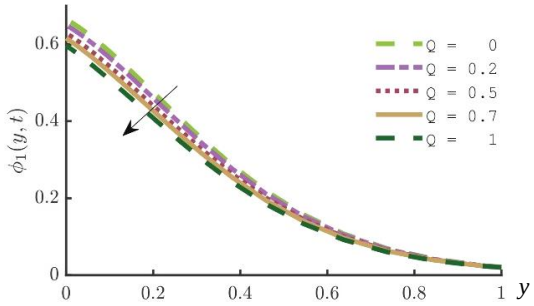

Figure 17. Impact of Q on temperature.

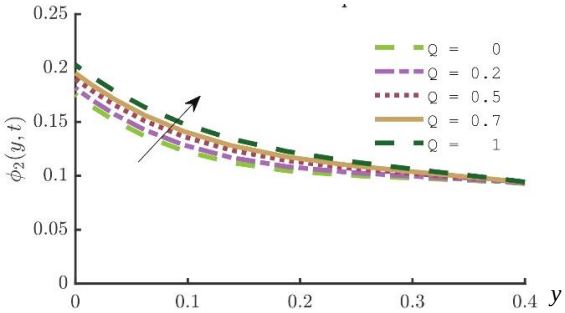

Figure 18. Impact of Q on concentration field.

Activation energy signifies a small amount of energy that causes a transformation or chemical reaction, augments nanoparticle concentration (Fig. 19). The potential for reaction rate is increased by activation energy, which also increases the nanoparticle concentration in the boundary layer region.

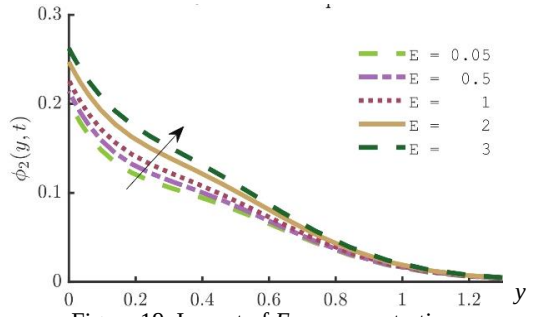

Figure 19. Impact of E on concentration.

Response of time on fluid velocity, temperature, and concentration is summarised in Figs. 20-22. It is delineated from Figs. 20-22 that momentum, thermal, and concentration boundary layer develops with time. The time has an enhancing nature on fluid velocity, temperature, and nanoparticle concentration. The values of heat transfer coefficient (Nusselt number) and mass transfer coefficient (Sherwood number) are depicted in Table 1 for varying the modified Lorentz force, Prandtl number, Eckert number, and thermal and solutal Biot number.

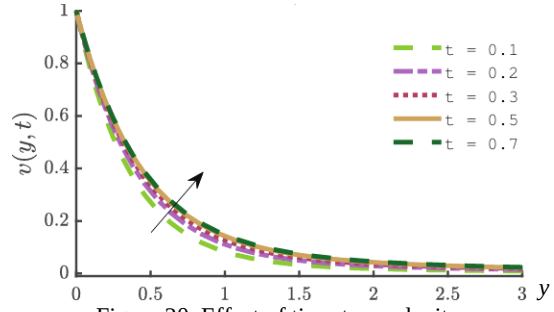

Figure 20. Effect of time t on velocity.

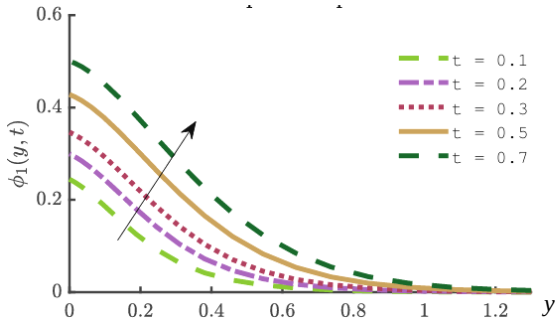

Figure 21. Effect of time t on temperature.

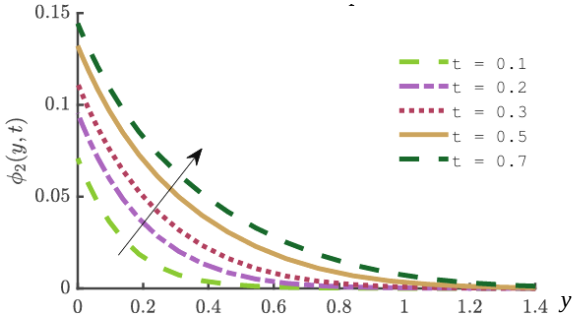

Figure 22. Effect of time t on concentration.

Table 1. Impact of Q, Pr, Ec, Γ_1, and Γ_2 on Nu_x (Nusselt number) and Sh_x (Sherwood number).

Q	Pr	Ec	Γ_1	Γ_2	Nu_x	Sh_x
1	12	0.2	2	1	0.786042	0.786767
2					0.866916	0.766515
3					0.966547	0.749551
	2				0.595822	0.794169
	4				0.692376	0.788361
	6				0.793691	0.786285
		0			1.106348	0.713762
		0.1			0.946944	0.750804
		0.2			0.786042	0.786767
			1		0.573107	0.870261
			2		0.786042	0.786767
			3		0.898032	0.782075
				1	0.786042	0.786767
				2	0.756241	1.331982
				3	0.733173	1.728639

CONCLUSION

Transient Jeffery nanofluid flow over a surface, capable of manifesting electromagnetic hydrodynamic behaviour is explored. Impulsive movement of the Riga plate is accounted. Heat transfers are simulated by incorporating the combined effects of a magnetic field, a modified Lorentz force, viscous dissipations, thermophoresis, Brownian motion, and convective boundary conditions. The spectral quasilinearization method is implemented to generate approximate solutions of partial differential equations representing the flow system. MATLAB® is used to run the code of numerical scheme. Impacts of selected parameters are studied. By assessing the solution and residual error norms, convergence of the method and accuracy of obtained solutions are substantiated. The solution error norms show a decline in the error until convergence takes place, verifying the convergence of the approach. Residual error norms indicate that the approximate solutions generated using the SQLM approach are accurate. The following key results are deduced from this study:

- β has a decreasing influence on fluid velocity.
- Fluid temperature and nanoparticle concentration increase with the thermal Biot number.
- Temperature and concentration profiles intensify with an increase in the solutal Biot number.
- An inverse relation of the modified Hartmann number with the temperature profile is observed. Velocity and concentration profiles increase with an increment in the modified Hartmann number.
- The concentration profile improves with a rise in the Arrhenius activation energy parameter.
- With the increase in time, the fluid velocity, temperature, and concentration profiles augment.

REFERENCES

1. Gupta, S., Kumar, D., Singh, J. (2018), *MHD mixed convective stagnation point flow and heat transfer of an incompressible nanofluid over an inclined stretching sheet with chemical reaction and radiation*, Int. J Heat Mass Transf. 118: 378-387. doi: 10.1016/j.ijheatmasstransfer.2017.11.007
2. Shafiq, A., Zari, I., Rasool, G., et al. (2019), *On the MHD Casson axisymmetric Marangoni forced convective flow of nanofluids*, Math. 7(11): 1087. doi: 10.3390/math7111087
3. Rasool, G., Zhang, T. (2019), *Darcy-Forchheimer nanofluidic flow manifested with Cattaneo-Christov theory of heat and mass flux over non-linearly stretching surface*, PLoS ONE, 14(8): e0221302. doi: 10.1371/journal.pone.0221302
4. Rasool, G., Zhang, T., Shafiq, A. (2019), *Marangoni effect in second grade forced convective flow of water based nanofluid*, J Adv. Nanotechnol. 1(1): 50-61. doi: 10.14302/issn.2689-2855.jan-19-2716
5. Lund, L.A., Omar, Z., Khan, I., et al. (2019), *Stability analysis of Darcy-Forchheimer flow of Casson type nanofluid over an exponential sheet: Investigation of critical points*, Symmetry, 11(3): 412. doi: 10.3390/sym11030412
6. Nayak, M.K., Oyelakin, I.S., Mondal, S., Sen, S.S. (2019), *Impact of the Cattaneo-Christov thermal and solutal diffusion models on the stagnation point slip flow of Walters' B nanofluid past an electromagnetic sheet*, Heat Transfer-Asian Res. 48(2): 713-726. doi: 10.1002/htj.21402
7. Meenakumari, R., Lakshminarayana, P., Vajravelu, K. (2021), *Unsteady MHD flow of a Williamson nanofluid on a permeable stretching surface with radiation and chemical reaction effects*,

Eur. Phys. J Spec. Top. 230: 1355-1370. doi: 10.1140/epjs/s11734-021-00039-7
8. Trivedi, M., Otegbeye, O., Ansari, M.S., Fayaz, T. (2023), *Flow of Jeffrey fluid near impulsively moving plate with nanoparticle and activation energy*, Int. J Thermofluids, 18: 100354. doi: 10.1016/j.ijft.2023.100354
9. Kumar, Y.S., Hussain, S., Raghunath, K., et al. (2023), *Numerical analysis of magnetohydrodynamics Casson nanofluid flow with activation energy, Hall current, and thermal radiation*, Sci. Rep. 13: 4021. doi: 10.1038/s41598-023-28379-5
10. Gailitis, A.K., Lielausis, O.A. (1961), *On the possibility of drag reduction of a flat plate in an electrolyte*, Appl. Magnetohydrodyn. Trudy Inst. Fisiky AN Latvia SSR, 12, p.143.
11. Hayat, T., Abbas, T., Ayub, M., et al. (2016), *Flow of nanofluid due to convectively heated Riga plate with variable thickness*, J Mol. Liq. 222: 854-862. doi: 10.1016/j.molliq.2016.07.111
12. Rasool, G., Zhang, T., Shafiq, A. (2019), *Second grade nanofluidic flow past a convectively heated vertical Riga plate*, Phys. Scr. 94(12): 125212. doi: 10.1088/1402-4896/ab3990
13. Shamshuddin, M.D., Narayana, P.V. (2020), *Combined effect of viscous dissipation and Joule heating on MHD flow past a Riga plate with Cattaneo-Christov heat flux*, Ind. J Phys. 94(9): 1385-1394. doi: 10.1007/s12648-019-01576-7
14. Hakeem, A.K.A., Ragupathi, P., Saranya, S., Ganga, B. (2020), *Three dimensional non-linear radiative nanofluid flow over a Riga plate*, J Appl. Comput. Mech. 6(4): 1012-1029. doi: 10.22055/jacm.2019.30095.1678
15. Ragupathi, P., Hakeem, A.K.A., Al-Mdallal, Q.M., et al. (2019), *Non-uniform heat source/sink effects on the three-dimensional flow of Fe_3O_4/Al_2O_3 nanoparticles with different base fluids past a Riga plate*, Case Stud. Therm. Eng. 15: 100521. doi: 10.1016/j.csite.2019.100521
16. Iqbal, Z., Azhar, E., Mehmood, Z., Maraj, E.N. (2017), *Melting heat transport of nanofluidic problem over a Riga plate with erratic thickness: Use of Keller Box scheme*, Results Phys. 7: 3648-3658. doi: 10.1016/j.rinp.2017.09.047
17. Ahmad, R., Mustafa, M., Turkyilmazoglu, M. (2017), *Buoyancy effects on nanofluid flow past a convectively heated vertical Riga-plate: A numerical study*, Int. J Heat Mass Transf. 111: 827-835. doi: 10.1016/j.ijheatmasstransfer.2017.04.046
18. Ganesh, N.V., Al-Mdallal, Q.M., Fahel, S.A., Dadoa, S. (2019), *Riga - plate flow of Al_2O_3-water/ethylene glycol with effective Prandtl number impacts*, Heliyon, 5(5): e01651. doi: 10.1016/j.heliyon.2019.e01651
19. Hakeem, A.K.A., Ganesh, N.V., Ganga, B. (2015), *Heat transfer of non-Darcy MHD flow of nanofluid over a stretching/shrinking surface in a thermally stratified medium with second order slip model*, Scientia Iranica, Trans. F Nanotechnol. 22(6): 2766-2784.
20. Ganesh, N.V., Hakeem, A.K.A., Ganga, B. (2018), *Darcy-Forchheimer flow of hydromagnetic nanofluid over a stretching/shrinking sheet in a thermally stratified porous medium with second order slip, viscous, and Ohmic dissipations effects*, Ain Shams Eng. J, 9(4): 939-951. doi: 10.1016/j.asej.2016.04.019
21. Ahmad, A., Asghar, S., Afzal, S. (2016), *Flow of nanofluid past a Riga plate*, J Magn. Magn. Mater. 402: 44-48. doi: 10.1016/j.jmmm.2015.11.043
22. Islam, M.M., Khatun, S., Mollah, M.T., Alam, M.M. (2021), *Fluid flow along the Riga plate with the influence of magnetic force in a rotating system*, arXiv:2103.14034. doi: 10.48550/arXiv.2103.14034
23. Rooman, M., Jan, M.A., Shah, Z., et al. (2021), *Entropy optimization and heat transfer analysis in MHD Williamson nanofluid flow over a vertical Riga plate with nonlinear thermal radiation*, Sci. Rep. 11: 18386. doi: 10.1038/s41598-021-97874-4
24. Kalaivanan, R., Ganesh, N.V., Al-Mdallal, Q.M. (2021), *Buoyancy driven flow of a second-grade nanofluid flow taking into account the Arrhenius activation energy and elastic deformation: Models and numerical results*, Fluid Dyn. Mater. Process. 17 (2): 319-332. doi: 10.32604/fdmp.2021.012789
25. Nasir, S., Berrouk, A.S., Gul, T. (2023), *Unsteady mix convectional stagnation point flow of nanofluid over a movable electromagnetohydrodynamics Riga plate numerical approach*, Sci. Rep. 13: 10947. doi: 10.1038/s41598-023-37575-2
26. Alhowaity, A., Mehmood, Y., Hamam, H., Bilal, M. (2023), *Radiative flow of nanofluid past a convected vertical Riga plate with activation energy and nonlinear heat generation*, Proc. Inst. Mech. Eng. Part E: J Process. Mech. Eng. 237(5): 1799-1807. doi: 10.1177/09544089221126439
27. Algehyne, E.A., Saeed, A., Arif, M., et al. (2023), *Gyrotactic microorganism hybrid nanofluid over a Riga plate subject to activation energy and heat source: numerical approach*, Sci. Rep. 13: 13675. doi: 10.1038/s41598-023-27562-y
28. Ali, A., Ahmed, M., Ahmad, A., Nawaz, R. (2023), *Enhanced heat transfer analysis of hybrid nanofluid over a Riga plate: Incorporating Lorentz forces and entropy generation*, Tribol. Int. 188: 108844. doi: 10.1016/j.triboint.2023.108844
29. Riaz, M., Khan, N., Hashmi, M.S., Younis, J. (2023), *Heat and mass transfer analysis for magnetized flow of ZnO-SAE50 nanolubricant with variable properties: an application of Cattaneo-Christov model*, Sci. Rep. 13: 8717. doi: 10.1038/s41598-023-35988-7
30. Ansari, M.S., Magagula, V.M., Trivedi, M. (2020), *Jeffrey nanofluid flow near a Riga plate: Spectral quasilinearization approach*, Heat Transf. 49(3): 1491-1510. doi: 10.1002/htj.21673
31. Ramanjini, V., Krishna, G.G., Mishra, S.R., et al. (2022), *An unsteady axisymmetric Williamson nanofluid flow over a radially stretching Riga plate for the inclusion of mixed convection and thermal radiation*, Part. Differ. Eq. Appl. Math. 6: 100456. doi: 10.1016/j.padiff.2022.100456